HHS Public Access

Author manuscript

Nat Commun. Author manuscript; available in PMC 2014 December 28.

Published in final edited form as:

Nat Commun. ; 3: 617. doi:10.1038/ncomms1625.

Structural rearrangements underlying ligand-gating in Kir channels

Shizhen Wang[1,2], **Sun-Joo Lee**[1], **Sarah Heyman**[1], **Decha Enkvetchakul**[2], and **Colin G. Nichols**[1,*]

[1]Department of Cell Biology and Physiology and Center for Investigation of Membrane Excitability Diseases, Washington University School of Medicine, 425 S. Euclid Ave., St. Louis, MO 63110 USA

[2]Department of Pharmacological and Physiological Sciences, Saint Louis University, 1402 South Grand Blvd., St. Louis, MO 63104 USA

Abstract

Inward rectifier potassium (Kir) channels are physiologically regulated by a wide range of ligands that all act on a common gate, although structural details of gating are unclear. Here we show, using small molecule fluorescent probes attached to introduced cysteines, the molecular motions associated with gating of KirBac1.1 channels. The accessibility of the probes indicates a major barrier to fluorophore entry to the inner cavity. Changes in FRET between fluorophores attached to KirBac1.1 tetramers show that PIP_2-induced closure involves tilting and rotational motions of secondary structural elements of the cytoplasmic domain that couple ligand binding to a narrowing of the cytoplasmic vestibule. The observed ligand-dependent conformational changes in KirBac1.1 provide a general model for ligand-induced Kir channel gating at the molecular level.

Inward rectifier potassium (Kir) channels are encoded by members of a major structural K channel family. Each subunit contains a unique cytoplasmic 'Kir' domain, formed by the N- and extensive C- termini, through which these channels are physiologically regulated by a wide range of ligands[1, 2]. For example, Kir1.x is gated by intracellular pH[3, 4], Kir3.x (GIRKs) is opened by Gβγ subunits[5, 6], while Kir6.x (K_{ATP}) is closed by ATP[7]. All eukaryotic Kir channels share a common activatory ligand, PIP_2, which again acts through binding to the Kir domain[8–10]. Despite the physiological significance of ligand gating, the molecular motions associated with ligand-induced gating remain unclear.

*Corresponding Author: Department of Cell Biology and Physiology and Center for Investigation of Membrane Excitability Diseases, Washington University School of Medicine, 425 S. Euclid Ave., St. Louis, MO 63110 USA, Tel: 1-314-362-6630, Fax: 1-314-362-2244, cnichols@wustl.edu.

Author contributions statements

SW, SJL, DE and CGN designed the study, SW, SJL, DE and SH performed experiments and analysis, SW, SJL and CGN wrote the paper.

Competing financial interests

The authors declare no competing financial interests.

A class of prokaryotic Kir channel homologs, referred to as KirBac channels, have also been identified and characterized[11–14], and crystal structures of full-length prokaryotic KirBac1.1 and eukaryotic Kir2.2 were first obtained in 2003 and 2009, respectively[15, 16]. Kir channel crystal structures share high similarity to other K channel structures in the transmembrane regions, but are unique within the 'Kir' cytoplasmic domain[15–17]. Both eukaryotic Kir and KirBac channels therefore contain the appropriate 'Kir' domain for ligand-gating, although, in striking contrast to all eukaryotic Kir channels, KirBac1.1 is inhibited by PIP_2[13, 18, 19], potentially due to key structural differences in the linkers between the Kir domain and the transmembrane domains[8, 19, 20]. There is accumulating evidence that gating in many K channels, including inward rectifiers, requires a bending/rotating motion of the pore-forming transmembrane α-helices to remove the bundle crossing gate[21–26]. For KcsA, neutralization of negatively charged residues at acidic pH enhances the repulsion contributed by positively charged residues clustered at the bundle crossing, thereby stabilizing the channel in the open state[27–29]. Molecular dynamics simulations, mass spectrometric measurements, AFM techniques and GFP-based FRET approaches have also provided data consistent with the interpretation that ligand-dependent opening of Kir channels involves opening of the bundle crossing gate and rearrangement of the cytosolic domain[24, 30–32]. Irrespective of where the ligand-operated gate is actually located, such studies have provided no information on the molecular motions of the Kir domain that underlie the gating, i.e. the molecular motions that are induced by ligand binding.

Recently, Clarke et al[33] presented 11 KirBac3.1 crystal structures that demonstrate differences in ion occupancies within the selectivity filter, and differences within the cytosolic domain. The authors proposed a gating mechanism at the selectivity filter mediated by interaction between the cytoplasmic domain and the slide helix, although none of these structures actually demonstrate an opening of the bundle crossing that could support conduction, and it is not clear how the structural variants that are observed actually relate to gating states[34].

In the present work we set out to examine gating motions within the KirBac1.1 channel protein that are definitively associated with ligand-gating, using PIP_2 as a ligand to drive channel closure. The data demonstrate specific motions of Kir domain β-sheets that result in narrowing of the cytoplasmic pore during PIP_2-induced closure.

Results

A major pore barrier at the bundle crossing

Wild type KirBac1.1 contains no cysteines (Supplementary Fig. S1) and thus provides a suitable model system for the introduction of cysteines that can be labeled with fluorescent tags. We first tested accessibility of substituted cysteines at different positions within the channel pore to Alexa Fluor 488 C5 maleimide (AF-488). The results (Fig. **1a,c**) show that all substituted cysteines up to and including residue 150C are rapidly modified, indicating no barrier to the relatively bulky AF-488. There is only very slow modification of residues A147C and F149C, and no modification by AF-488 of cysteine residues that are actually within the inner cavity (A109C, T110C, I138C, T142C, G143C, V145C and F146C). In addition to a major restriction at the bundle crossing (immediately above residue 150),

eukaryotic Kir crystal structures have revealed a secondary constriction at the so-called G-loop (that includes residue 264, Fig. **1e**), located just below the bundle crossing[35–37]. Our results indicate a major restriction at the bundle crossing, whereas the G-loop provides no detectable barrier to access of AF-488.

As discussed above, PIP_2 has an inhibitory effect on KirBac1.1 channel activity[13, 19], and modification rates of pore-lining cysteines within the cytoplasmic vestibule all dropped ~15% in the presence of 10 μg/ml diC8-PIP_2 (Fig. **1b,d**). Interestingly, the modification rate was even greater slower (~30%) at residue 180C which is located on the outer wall of the cytosolic domain. This residue is close to PIP_2 binding sites recently identified in Kir2.2 and Kir3.2 by crystallography[8, 35], and potentially the reduced accessibility reflects shielding of 180C as a consequence of diC8-PIP_2 binding.

KirBac1.1 cysteine mutants are functional and PIP_2 sensitive

Random labeling of mutant proteins with cysteine-reactive FRET donor/acceptor mixtures allows us to measure the gating-associated motions of labeled cysteines induced by PIP_2. In the present work, cysteine residues were introduced at 21 different positions throughout the KirBac1.1 cytoplasmic domain (Supplementary Fig. S1) and randomly labeled by EDANS C2 maleimide/DABCYL-plus C2 maleimide (E/D, R_0 = 33 Å) or Alexa-Fluor-546 C5 maleimide/DABCYL-plus C2 maleimide (A/D, R_0 = 29 Å). We previously showed that wild type KirBac1.1 in POPE/POPG (3:1) liposomes has high intrinsic open probability, but channel open probability is dramatically decreased by low levels of PIP_2[13, 19]. We examined the channel activity, and PIP_2-sensitivity, of fluorophore-labeled KirBac1.1 cysteine mutants using a rubidium flux assay. Most fluorophore-labeled mutants are functional and remain sensitive to PIP_2 inhibition (Fig 2). Four mutants, including 177-AD, 186-AD, 228-AD and 306-ED were non-functional. Among these, 177-AD is apparently a consequence of the labeling, since 177-ED is still functional and PIP_2 sensitive. Residue 228 is located in the middle of the major β-sheet (βI, see below), while 186 is located at a subunit interface, and 306 is located at the extreme C-terminal end of the protein, in a small β-sheet region that is conserved among Kir channel members (Supplementary Fig S1). Structurally, these residues are all located far from the membrane interface and are unlikely to be involved in PIP_2 binding. Mutation and fluorophore-labeling may break their interactions with other residues, or block the ion conduction pathway, and the relevance of any PIP_2-induced conformational changes at these sites to gating transitions therefore needs to be considered carefully (see Discussion). We also noticed that 219C-AD is active but loses PIP_2 sensitivity. This residue is located in a connecting loop, and mutation or labeling may disrupt transduction of PIP_2-triggered conformational changes, preventing closure of the channel pore (Fig 2). Interestingly, and consistent with this interpretation, this residue showed only minimal PIP_2-dependent changes in FRET (see below).

Movements of individual residues during PIP_2-induced gating

In order to investigate the gating-associated motions of the KirBac1.1 cytoplasmic domain, 21 cysteine mutants, labeled with E/D or A/D FRET pairs, were reconstituted into POPE/POPG (3:1) liposomes with or without 1.25% PIP_2 and apparent FRET efficiencies were measured as described in the Methods. Unlabeled mutant protein reconstituted into

liposomes was used as a control to subtract background fluorescence. Proteinase K was used to digest the protein and break the fluorescence resonance energy transfer pathway, thereby allowing measurement of maximum donor emissions (Fig. **3a**) after 5–60 minutes. Four mutants were tested with both A/D and E/D pairs. In each case, the directional change of FRET was the same, although there were large differences in individual FRET efficiencies, which may be due to different R_0 of the FRET pairs, as well as the size and orientation of fluorophores (Table 1). Predicted FRET efficiencies were calculated from absolute distances between residues in KirBac1.1 crystal structures (2WLL, 1P7B), assuming two- or four-fold symmetry (Methods and Supplementary Table S1). There was a significant correlation between FRET-reported inter-subunit distances and distances predicted by the KirBac1.1 crystal structure (2WLL) (Fig. 3**b**). Although the 2WLL crystal structure actually exhibits a slight two-fold symmetry, the correlation was essentially identical whether the measured FRET efficiencies were compared to the predicted efficiencies with either two fold (a≠b) or four fold symmetry (a=b, Supplementary Fig. S2).

There is a good overall correlation between the FRET-reported distances and those predicted by the crystal structure (Fig. **3b**). There is a systematic deviation in reported distances for E/D versus A/D pairs, i.e. E/D reports wider distances (~20 Å), when both pairs are examined at the same residue. The side chains of these residues (165, 177, 249, 273) all potentially orient towards the pore axis in the KirBac1.1 crystal structure. Since the spacer arm of EDANS is shorter than that of Alexa-Fluor 546 (by >10 Å), the A/D pair will report shorter distances than the E/D pair. There is significant deviation between FRET reported distances and crystallographic predictions at two residues in particular, 165C-AD and 308C-AD. Residue 308 is located at the outside edge of the cytoplasmic domain, and we suggest that the lack of correlation may be a result of the flexible nature of this region or the relative orientation of fluorophores within the tetramer. The latter interpretation seems potentially correct for 165C; while the FRET-reported distance for 165C-AD is considerably less than that predicted from 2WLL, the 165C-ED-reported distance is actually well correlated (Fig. 3**b**) and, moreover, 165C-ED is functionally much more active than 165C-AD (Fig.2), suggesting a disruptive consequence of AD modification. Interestingly, measured FRET efficiencies in the presence of PIP_2 show slightly better correlation with predicted FRET efficiencies from the KirBac1.1 crystal structure, consistent with the crystal structure being in a closed state.

Residue motions suggest movements of secondary structures

The KirBac1.1 cytoplasmic domain consists of two major β-sheets, one (which we refer to as βI, including residues 186, 191, 252, 258, 260, 264, 273, Fig. 4**a**) that is tilted ~45° relative to the membrane plane, and a second (βII, including residues 165, 177, 225, 228, Fig.4**c**), that is approximately parallel with the pore axis. Small, but reproducible differences in FRET efficiencies (up to 15%), were detected for most residues in the presence and absence of PIP_2 (Table 1). Comparison of FRET efficiencies in the presence (closed) and absence (open) of PIP_2 reveals important consistencies. First, in the presence of PIP_2, all residues located at the top ends of βI move inwards relative to the central axis (264C, 260C, 258C, 186C and 191C), while residues at the bottom ends of βI (252C and 273C) and their attached short α-helix (249C and 277C) and β-sheets (280C and 283C) all move outwards.

These data suggest a tilt motion of βI during PIP_2-induced channel closure, with the top ends bending towards- and bottom ends bending away- from the pore axis (Fig. 4**a,b**). Second, all of the tested residues in βII and the associated loops and short helical stretches (219C, 225C, 228C, 235C, 180C, 177C, 165C, 306C and 308C) move inwards in the presence of PIP_2, consistent with this whole region moving as a unit (Fig. **4c,d**). Third, all cytoplasmic pore-lining residues (151, 264, 260, 258, 186, 191, 219, 235), showed increased FRET efficiencies in the presence of PIP_2, indicating that the cytoplasmic vestibule narrows throughout in the closed state (Fig. 4), consistent with accessibility data (Fig. 1).

Discussion

The growing number of K channels for which crystal structures are available (including KcsA[17], MthK[21], KvAP[38], KirBac1.1[15], Kv1.2[39], NaK[40, 41] and Kir2.2[16]) indicate that transmembrane domain structures are highly conserved. Crystallization of MthK in an open state provided the first direct view of an open K channel[21], and revealed that removal of the major hydrophobic gate at the bundle crossing occurred by bending of pore forming α-helices away from the pore axis[21, 22]. Similar structural changes have since been observed with open state crystal structures of KcsA[42, 43] and NaK[41]. For Kir and KirBac channels, there is also strong evidence for ligand-gating occurring at or near the bundle crossing[25, 26, 44, 45]. Our accessibility data indicate a significant barrier to fluorophore accessibility at the bundle crossing (F146), with enhanced accessibility of A150C immediately beneath the bundle crossing, and no significant barrier below this level.

Rubidium flux assays indicate that PIP_2 significantly inhibits almost all labeled mutant channels (Fig. 2), and our FRET studies reveal movements of multiple residues in the cytoplasmic domain in the presence of PIP_2. In Rb flux assays, the potency of PIP_2 inhibition of labeled mutants ranges from ~40%–99% (Fig. 2), and in most cases, inhibition will be incomplete, such that FRET-reported movements between open- and closed-conformations will be underestimations. In addition, uncertainties of fluorophore orientation factors preclude exact determinations of distances, but the direction of motion at each residue revealed by FRET measurements will be relatively robust. The qualitative patterns of directional movement (relative to the central axis of the channel) that then emerge (Fig. 4) are consistent with essentially rigid body motions of the major secondary structural elements within the cytoplasmic Kir domain, similar to the proposal of Nishida et al based on observation of two distinct conformations of the KirBac1.3–Kir3.1 chimera cytoplasmic domain[46].

In order to visualize potential motions of the Kir domain, we generated ‘cartoon’ models for the open KirBac1.1 channel by modifying backbone coordinates of the closed KirBac1.1 (1P7B, Matlab, Mathworks Inc) in an attempt to match the constraints provided by the FRET measurements. Opening of the pore at the M2 helix bundle crossing was achieved by rotation and bending of TM2 at residue G134 (a potential hinge residue in K channels in general[21, 47]) and then coupled rigid body motion of the cytoplasmic domain was applied. The degree of bending of TM2, and rigid translation of the C-terminal domain were varied to minimize disagreement with the FRET data. The unknown orientation factors of the fluorophores and potential perturbation effects of mutations and chemical labeling severely

limit the resolution of the FRET measurements and prohibit unambiguous assessment of absolute distances, but the qualitative structural constraints obtained by FRET measurements are reasonably well met by the 'cartoon' open model shown in Fig. 5 (and Supplementary Movie 1). The model was generated by tilting of βI, with the top end moving away from, and the bottom end towards, the pore axis (***i***), which widens the upper end of the cytoplasmic vestibule, and anticlockwise twist of βII leads to changes in the subunit interfaces and movement of βII away from the central axis (***ii***), which widens the cytoplasmic pore. The directional movements indicated by the FRET measurements are replicated for 19 out of 21 residues (Table 1), and are consistent with results obtained from other biochemical and biophysical studies on Kir channel open state conformations[30, 44, 45], as well as predictions of molecular dynamic simulation studies[24, 47–49].

Eukaryotic and prokaryotic Kir channels have distinct and opposite responses to PIP_2: while KirBac1.1 is closed by PIP_2 binding, all eukaryotic Kir channels are opened by PIP_2. The different response to PIP_2 is likely to depend on critical differences in binding site orientation or on coupling of binding to the Kir domain gating machinery. Different structures of the loops that link the transmembrane and cytoplasmic domains constituting the PIP_2 binding pocket are likely to be important[15, 16]. Indeed a recently solved crystal structure of PIP_2-bound Kir2.2 indicates key interacting residues that are absent from the linker loop of KirBac1.1[8]. A second PIP_2-bound Kir3.2 structure reveals binding at a similar location[35] and, moreover, PIP_2 binding, which leads to channel activation in Kir3.2 channels, causes a twist in the major (β1) β-sheet that is qualitatively quite similar to that which we predict in the (PIP_2-unbound) 'open' KirBac1.1. The eukaryotic Kir family exhibits sensitivity to a remarkably broad range of cytoplasmic ligands that are all likely to converge on similar conformational responses. Each sub-family from Kir1 to Kir7 has been shown to be activated by PIP_2[50–56], and biophysical analyses demonstrate that the unique ligands for different sub-families (pH in Kir1 and Kir4, Na and G-protein βγ subunits in Kir3, ATP in Kir6) are convergent on the same process, such that kinetic models of gating implicitly involve the same gate as that activated by PIP_2. This leads us to speculate that open-closed motions that we detect in the present study will be replicated in the ligand-induced gating of all eukaryotic inward rectifiers.

Methods

DNA manipulation and protein expression

DNA manipulation, expression and purification of KirBac1.1 cysteine substitution mutants, are essentially as described previously[12, 19, 57] except for changing the gel filtration buffer to 20 mM HEPES with 150 KCl and 5 mM DM, pH 7.5. Tetramer fractions were collected and concentrated to 3mg/ml for chemical labeling with the maleimide form of fluorophore pairs. Cysteine-substituted KirBac1.1 mutants were labeled with EDANS C2 maleimide/ DABCYL-plus C2 maleimide (E/D, ANASPEC), at protein:E:D ratio of 1:10:10, or with Alexa-Fluor-546 C5 maleimide (Invitrogen)/DABCYL-plus C2 maleimide (A/D) at a protein:A:D ratio of 1:2.5:10. Labeling reactions were performed at room temperature for 1 hr then proteins were loaded onto a 5 ml Hitrap desalting column (GE Healthcare) to remove

free probe. Labeled protein samples were collected and concentrated to 1.0 mg/ml (KirBac1.1-A/D) or 3.0 mg/ml (KirBac1.1-E/D) for reconstitution.

Accessibility assay using Alexa Fluor 488 C5 maleimide

Accessibility assays were performed at room temperature using labeling buffer containing ~400–500ng of KirBac1.1 in labeling buffer (20 mM Hepes, 150 mM KCl, 5 mM DM, pH7.5) were immobilized on His-Sorb plates (Qiagen), then the assay was started by adding AF-488 at final protein:probe ratio of 1:50, in the presence or absence of 10 μg/ml of diC8-PIP_2. Free probes were removed by washing with labeling buffer (3×) and incorporation of AF-488 was monitored by emission at 525 nm with excitation wavelength of 485 nm. KirBac1.1 wild type protein was used as control to estimate and subtract nonspecific labeling.

Reconstitution of labeled KirBac1.1 into liposomes

Lipids (3:1 phosphatidylethanolamine (POPE):phosphatidylglycerol (POPG), Avanti Polar Lipids) were solubilized in buffer A (150 mM KCl, 20 mM HEPES, pH 7.5) containing 37 mM CHAPS with or without 1.25% phosphatidylinositol-4,5-bisphosphate (PIP_2) (w/w). The KirBac1.1 cysteine mutants form tetrameric proteins with one cysteine in each monomer. Combinatorially, labeling with E/D or A/D FRET pairs gives 6 different configurations of donor and acceptor labels, 4 of which will have at least one donor and acceptor within a given tetramer (Supplementary Table S1). The lipids were mixed with fluorophore-labeled protein at a ratio of 100:3 for KirBac1.1-E/D and 100:1 for KirBac1.1-A/D. The lipid/protein mixture was incubated for 20 min at room temperature, and then loaded onto a Sephadex G-50 column pre-equilibrated with buffer A to remove CHAPS and to obtain reconstituted proteoliposomes.

FRET Measurements

FRET experiments were performed using a Synergy 2 fluorescence reader with excitation/emission wavelengths of 360/460 nm for KirBac1.1-E/D and 540/570 nm for KirBac1.1-A/D. Following 8 repeated readings, proteinase K solution was added to the proteoliposome sample at a final concentration of 0.08 U/well. Fluorescence was monitored until reaching a new stable plateau. Unlabeled protein samples were reconstituted into liposomes with or without PIP_2 as controls to measure background fluorescence intensities. Fluorescence emission was measured before (F_o) and after proteinase digestion (F_{max}). The apparent FRET efficiency (E_{app}) is then given by the ratio of the quenched donor emission to the maximum donor emission:

$$E_{app}=(\mathrm{F_{max}}-\mathrm{F_o})/\mathrm{F_{max}}$$

Rubidium flux assay

Fluorophore-labeled KirBac1.1 cysteine mutants were reconstituted into liposomes containing 3:1 POPE:POPG with or without 1.25% PIP_2, at protein:lipid ratio of 1:100, as described by Enkvetchakul et al[12, 19]. The KCl concentration inside and outside of the liposome was 450 mM and 50 mM, respectively. Rubidium uptake over 15 min was

measured and normalized to valinomycin-dependent maximum uptake. All data are presented as mean±S.E from 3 independent repeats.

Data analysis

For fluorescence measurements, data are expressed as mean±S.E of multiple independent labeling and reconstitution experiments. Error propagation was used to calculate S.E. in Fig. 4. For calculating the apparent FRET efficiencies predicted by the crystal structure of KirBac1.1 (2WLL, or the 'open' structure model) in Table 1 and supplementary Fig S2, the distances between α-carbon of FRET measured residues at two adjacent subunits were used. For a tetramer with multiple donor and acceptor present, apparent FRET efficiencies (E_{app}) were calculated based on resonance energy transfer rate theory as described in detail by Cheng et al[58] (see Supplementary Table S1) using the following equation:

$$E_{app}=\frac{\sum_{n=0}^{4} n \cdot p_{D_n A_{4-n}} \cdot E^{D}_{D_n A_{4-n}}}{\sum_{n=0}^{4} n \cdot p_{D_n A_{4-n}}}$$

with the assumption that both donor and acceptor fluorophores are randomly incorporated into the KirBac1.1 tetramer. The Cα distance predicted by experimentally measured apparent FRET efficiencies in Fig. 3**b** were obtained using the same FRET model by setting a=b. (Supplementary Table S1).

Supplementary Material

Refer to Web version on PubMed Central for supplementary material.

Acknowledgements

We thank Dr. Beth Cotner-Gohara and Shawn Yackly for their technical support in using the Synergy2 reader, Dr. Nazzareno D'Avanzo and Wayland W.L. Cheng for constructive discussions. This work was supported by NIH grants HL54171 and HL45742 (to C.G.N), DK069424 (to D.E) and American Heart Association postdoctoral fellowship 10POST4280056 (to S.W).

References

1. Jan LY, Jan YN. Voltage-gated and inwardly rectifying potassium channels. J Physiol. 1997; 505(Pt 2):267–282. [PubMed: 9423171]
2. Nichols CG, Lopatin AN. Inward rectifier potassium channels. Annual review of physiology. 1997; 59:171–191.
3. McNicholas CM, et al. pH-dependent modulation of the cloned renal K+ channel, ROMK. The American journal of physiology. 1998; 275:F972–981. [PubMed: 9843915]
4. Schulte U, Hahn H, Wiesinger H, Ruppersberg JP, Fakler B. pH-dependent gating of ROMK (Kir1.1) channels involves conformational changes in both N and C termini. The Journal of biological chemistry. 1998; 273:34575–34579. [PubMed: 9852128]
5. Krapivinsky G, Krapivinsky L, Wickman K, Clapham DE. G beta gamma binds directly to the G protein-gated K+ channel, IKACh. The Journal of biological chemistry. 1995; 270:29059–29062. [PubMed: 7493925]
6. Reuveny E, et al. Activation of the cloned muscarinic potassium channel by G protein beta gamma subunits. Nature. 1994; 370:143–146. [PubMed: 8022483]

7. Nichols CG. KATP channels as molecular sensors of cellular metabolism. Nature. 2006; 440:470–476. [PubMed: 16554807]
8. Hansen SB, Tao X, MacKinnon R. Structural basis of PIP2 activation of the classical inward rectifier K+ channel Kir2.2. Nature. 2011; 477:495–498. [PubMed: 21874019]
9. Suh BC, Hille B. PIP2 is a necessary cofactor for ion channel function: how and why? Annu Rev Biophys. 2008; 37:175–195. [PubMed: 18573078]
10. Xiao J, Zhen XG, Yang J. Localization of PIP2 activation gate in inward rectifier K+ channels. Nat Neurosci. 2003; 6:811–818. [PubMed: 12858177]
11. Durell SR, Guy HR. A family of putative Kir potassium channels in prokaryotes. BMC evolutionary biology. 2001; 1:14. [PubMed: 11806753]
12. Enkvetchakul D, et al. Functional characterization of a prokaryotic Kir channel. The Journal of biological chemistry. 2004; 279:47076–47080. [PubMed: 15448150]
13. Cheng WW, Enkvetchakul D, Nichols CG. KirBac1.1: it's an inward rectifying potassium channel. The Journal of general physiology. 2009; 133:295–305. [PubMed: 19204189]
14. Sun S, Gan JH, Paynter JJ, Tucker SJ. Cloning and functional characterization of a superfamily of microbial inwardly rectifying potassium channels. Physiological genomics. 2006; 26:1–7. [PubMed: 16595742]
15. Kuo A, et al. Crystal structure of the potassium channel KirBac1.1 in the closed state. Science (New York, N.Y. 2003; 300:1922–1926.
16. Tao X, Avalos JL, Chen J, MacKinnon R. Crystal structure of the eukaryotic strong inward-rectifier K+ channel Kir2.2 at 3.1 A resolution. Science (New York, N.Y. 2009; 326:1668–1674.
17. Doyle DA, et al. The structure of the potassium channel: molecular basis of K+ conduction and selectivity. Science (New York, N.Y. 1998; 280:69–77.
18. D'Avanzo N, Cheng WW, Doyle DA, Nichols CG. Direct and specific activation Of human inward rectifier K+ channels by membrane phosphatidylinositol 4,5-bisphosphate. The Journal of biological chemistry. 2010; 285:37129–37132. [PubMed: 20921230]
19. Enkvetchakul D, Jeliazkova I, Nichols CG. Direct modulation of Kir channel gating by membrane phosphatidylinositol 4,5-bisphosphate. The Journal of biological chemistry. 2005; 280:35785–35788. [PubMed: 16144841]
20. D'Avanzo N, Cheng WW, Doyle DA, Nichols CG. Direct and specific activation of human inward rectifier K+ channels by membrane phosphatidylinositol 4,5-bisphosphate. J Biol Chem. 2010; 285:37129–37132. [PubMed: 20921230]
21. Jiang Y, et al. The open pore conformation of potassium channels. Nature. 2002; 417:523–526. [PubMed: 12037560]
22. Jiang Y, et al. Crystal structure and mechanism of a calcium-gated potassium channel. Nature. 2002; 417:515–522. [PubMed: 12037559]
23. Kuo A, Domene C, Johnson LN, Doyle DA, Venien-Bryan C. Two different conformational states of the KirBac3.1 potassium channel revealed by electron crystallography. Structure. 2005; 13:1463–1472. [PubMed: 16216578]
24. Haider S, Khalid S, Tucker SJ, Ashcroft FM, Sansom MS. Molecular dynamics simulations of inwardly rectifying (Kir) potassium channels: a comparative study. Biochemistry. 2007; 46:3643–3652. [PubMed: 17326663]
25. Phillips LR, Enkvetchakul D, Nichols CG. Gating dependence of inner pore access in inward rectifier K(+) channels. Neuron. 2003; 37:953–962. [PubMed: 12670424]
26. Phillips LR, Nichols CG. Ligand-induced closure of inward rectifier Kir6.2 channels traps spermine in the pore. The Journal of general physiology. 2003; 122:795–804. [PubMed: 14638936]
27. Cuello LG, Cortes DM, Jogini V, Sompornpisut A, Perozo E. A molecular mechanism for proton-dependent gating in KcsA. FEBS letters. 2010; 584:1126–1132. [PubMed: 20138880]
28. Thompson AN, Posson DJ, Parsa PV, Nimigean CM. Molecular mechanism of pH sensing in KcsA potassium channels. Proceedings of the National Academy of Sciences of the United States of America. 2008; 105:6900–6905. [PubMed: 18443286]

29. Miloshevsky GV, Jordan PC. Open-state conformation of the KcsA K+ channel: Monte Carlo normal mode following simulations. Structure. 2007; 15:1654–1662. [PubMed: 18073114]
30. Riven I, Kalmanzon E, Segev L, Reuveny E. Conformational rearrangements associated with the gating of the G protein-coupled potassium channel revealed by FRET microscopy. Neuron. 2003; 38:225–235. [PubMed: 12718857]
31. Grottesi A, Domene C, Haider S, Sansom MS. Molecular dynamics simulation approaches to K channels: conformational flexibility and physiological function. IEEE transactions on nanobioscience. 2005; 4:112–120. [PubMed: 15816177]
32. Lee JR, Shieh RC. Structural changes in the cytoplasmic pore of the Kir1.1 channel during pHi-gating probed by FRET. Journal of biomedical science. 2009; 16:29. [PubMed: 19272129]
33. Clarke OB, et al. Domain reorientation and rotation of an intracellular assembly regulate conduction in Kir potassium channels. Cell. 2010; 141:1018–1029. [PubMed: 20564790]
34. Zhou W, Jan LY. A twist on potassium channel gating. Cell. 2010; 141:920–922. [PubMed: 20550927]
35. Whorton MR, Mackinnon R. Crystal Structure of the Mammalian GIRK2 K(+) Channel and Gating Regulation by G Proteins, PIP(2), and Sodium. Cell. 2011; 147:199–208. [PubMed: 21962516]
36. Pegan S, et al. Cytoplasmic domain structures of Kir2.1 and Kir3.1 show sites for modulating gating and rectification. Nature neuroscience. 2005; 8:279–287. [PubMed: 15723059]
37. Nishida M, MacKinnon R. Structural basis of inward rectification: cytoplasmic pore of the G protein-gated inward rectifier GIRK1 at 1.8 A resolution. Cell. 2002; 111:957–965. [PubMed: 12507423]
38. Jiang Y, et al. X-ray structure of a voltage-dependent K+ channel. Nature. 2003; 423:33–41. [PubMed: 12721618]
39. Long SB, Campbell EB, Mackinnon R. Crystal structure of a mammalian voltage-dependent Shaker family K+ channel. Science (New York, N.Y. 2005; 309:897–903.
40. Shi N, Ye S, Alam A, Chen L, Jiang Y. Atomic structure of a Na+- and K+-conducting channel. Nature. 2006; 440:570–574. [PubMed: 16467789]
41. Alam A, Jiang Y. High-resolution structure of the open NaK channel. Nature structural & molecular biology. 2009; 16:30–34.
42. Cuello LG, Jogini V, Cortes DM, Perozo E. Structural mechanism of C-type inactivation in K(+) channels. Nature. 2010; 466:203–208. [PubMed: 20613835]
43. Cuello LG, et al. Structural basis for the coupling between activation and inactivation gates in K(+) channels. Nature. 2010; 466:272–275. [PubMed: 20613845]
44. Gupta S, et al. Conformational changes during the gating of a potassium channel revealed by structural mass spectrometry. Structure. 2010; 18:839–846. [PubMed: 20637420]
45. Paynter JJ, et al. Functional complementation and genetic deletion studies of KirBac channels: activatory mutations highlight gating-sensitive domains. The Journal of biological chemistry. 2010; 285:40754–40761. [PubMed: 20876570]
46. Nishida M, Cadene M, Chait BT, MacKinnon R. Crystal structure of a Kir3.1-prokaryotic Kir channel chimera. The EMBO journal. 2007; 26:4005–4015. [PubMed: 17703190]
47. Grottesi A, Domene C, Hall B, Sansom MS. Conformational dynamics of M2 helices in KirBac channels: helix flexibility in relation to gating via molecular dynamics simulations. Biochemistry. 2005; 44:14586–14594. [PubMed: 16262258]
48. Haider S, Grottesi A, Hall BA, Ashcroft FM, Sansom MS. Conformational dynamics of the ligand-binding domain of inward rectifier K channels as revealed by molecular dynamics simulations: toward an understanding of Kir channel gating. Biophysical journal. 2005; 88:3310–3320. [PubMed: 15749783]
49. Shrivastava IH, Capener CE, Forrest LR, Sansom MS. Structure and dynamics of K channel pore-lining helices: a comparative simulation study. Biophysical journal. 2000; 78:79–92. [PubMed: 10620275]
50. Huang CL, Feng S, Hilgemann DW. Direct activation of inward rectifier potassium channels by PIP2 and its stabilization by Gbetagamma. Nature. 1998; 391:803–806. [PubMed: 9486652]

51. Shyng SL, Nichols CG. Membrane phospholipid control of nucleotide sensitivity of KATP channels. Science (New York, N.Y. 1998; 282:1138–1141.

52. Sui JL, Petit-Jacques J, Logothetis DE. Activation of the atrial KACh channel by the betagamma subunits of G proteins or intracellular Na+ ions depends on the presence of phosphatidylinositol phosphates. Proceedings of the National Academy of Sciences of the United States of America. 1998; 95:1307–1312. [PubMed: 9448327]

53. Leung YM, Zeng WZ, Liou HH, Solaro CR, Huang CL. Phosphatidylinositol 4,5-bisphosphate and intracellular pH regulate the ROMK1 potassium channel via separate but interrelated mechanisms. The Journal of biological chemistry. 2000; 275:10182–10189. [PubMed: 10744702]

54. Schulze D, Krauter T, Fritzenschaft H, Soom M, Baukrowitz T. Phosphatidylinositol 4,5-bisphosphate (PIP2) modulation of ATP and pH sensitivity in Kir channels. A tale of an active and a silent PIP2 site in the N terminus. The Journal of biological chemistry. 2003; 278:10500–10505. [PubMed: 12514171]

55. Du X, et al. Characteristic interactions with phosphatidylinositol 4,5-bisphosphate determine regulation of kir channels by diverse modulators. The Journal of biological chemistry. 2004; 279:37271–37281. [PubMed: 15155739]

56. Rapedius M, et al. Long chain CoA esters as competitive antagonists of phosphatidylinositol 4,5-bisphosphate activation in Kir channels. The Journal of biological chemistry. 2005; 280:30760–30767. [PubMed: 15980413]

57. Wang S, Alimi Y, Tong A, Nichols CG, Enkvetchakul D. Differential roles of blocking ions in KirBac1.1 tetramer stability. The Journal of biological chemistry. 2009; 284:2854–2860. [PubMed: 19033439]

58. Cheng W, Yang F, Takanishi CL, Zheng J. Thermosensitive TRPV channel subunits coassemble into heteromeric channels with intermediate conductance and gating properties. The Journal of general physiology. 2007; 129:191–207. [PubMed: 17325193]

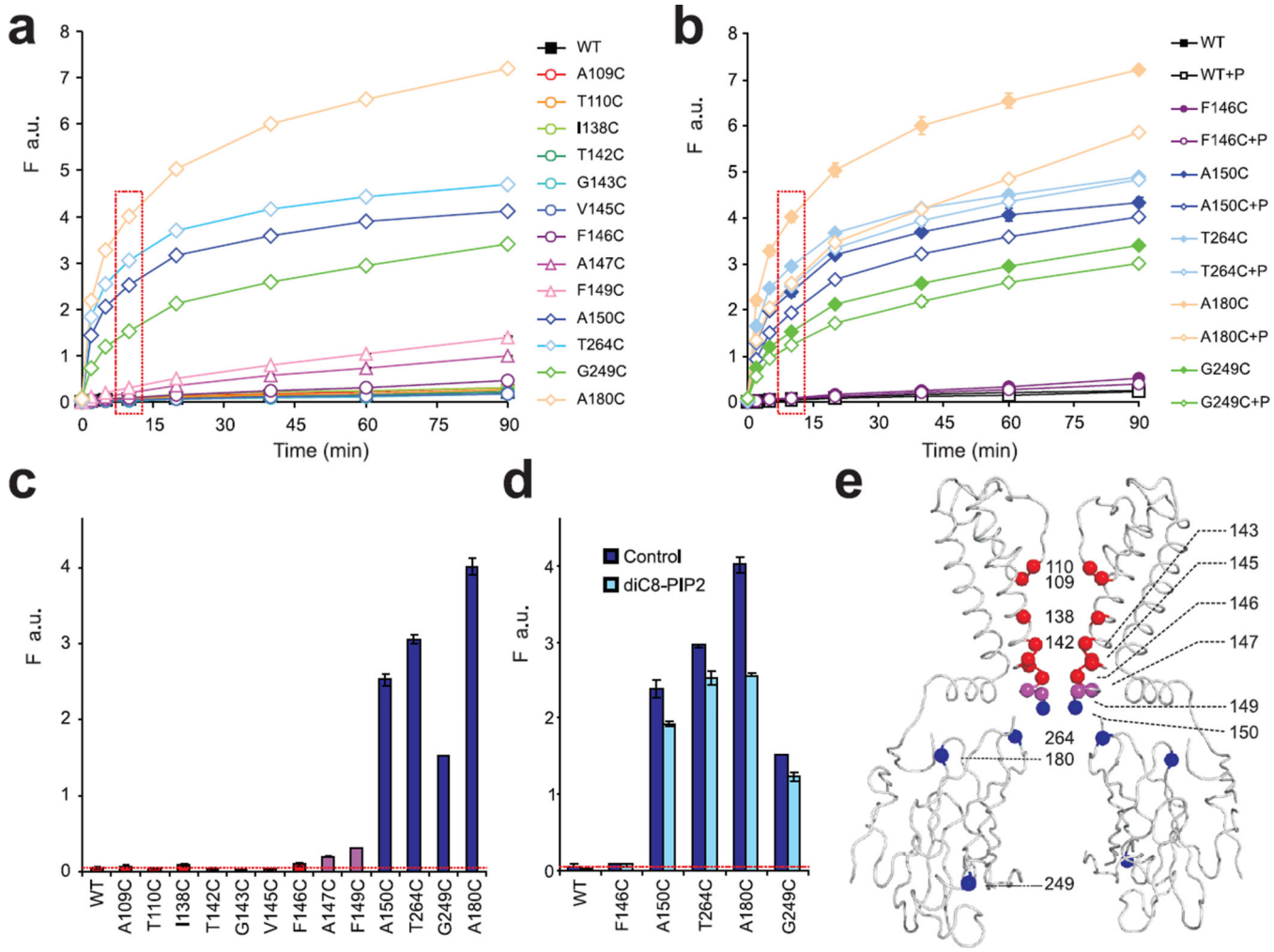

Fig. 1. Accessibility of KirBac1.1 channel pore lining residues

Time course (**a, b**) and 10 min time point data (**c, d**, boxed in **a, b**) of Alexa-Fluor 488 C5 maleimide incorporation (F, a.u.) of cysteine-substituted KirBac1.1 mutants in the presence or absence of 10 μg/ml diC8-PIP_2 (mean ± S.E., n=3 in each case, error bars are smaller than symbol in most cases) (**e**) Ribbon diagram indicating accessibility of AF-488 to substituted cysteine residues. Alpha carbons of tested residues in this and subsequent figures are highlighted by spheres, with inaccessible residues colored red, limited accessible (147 and 149) purple and highly accessible blue.

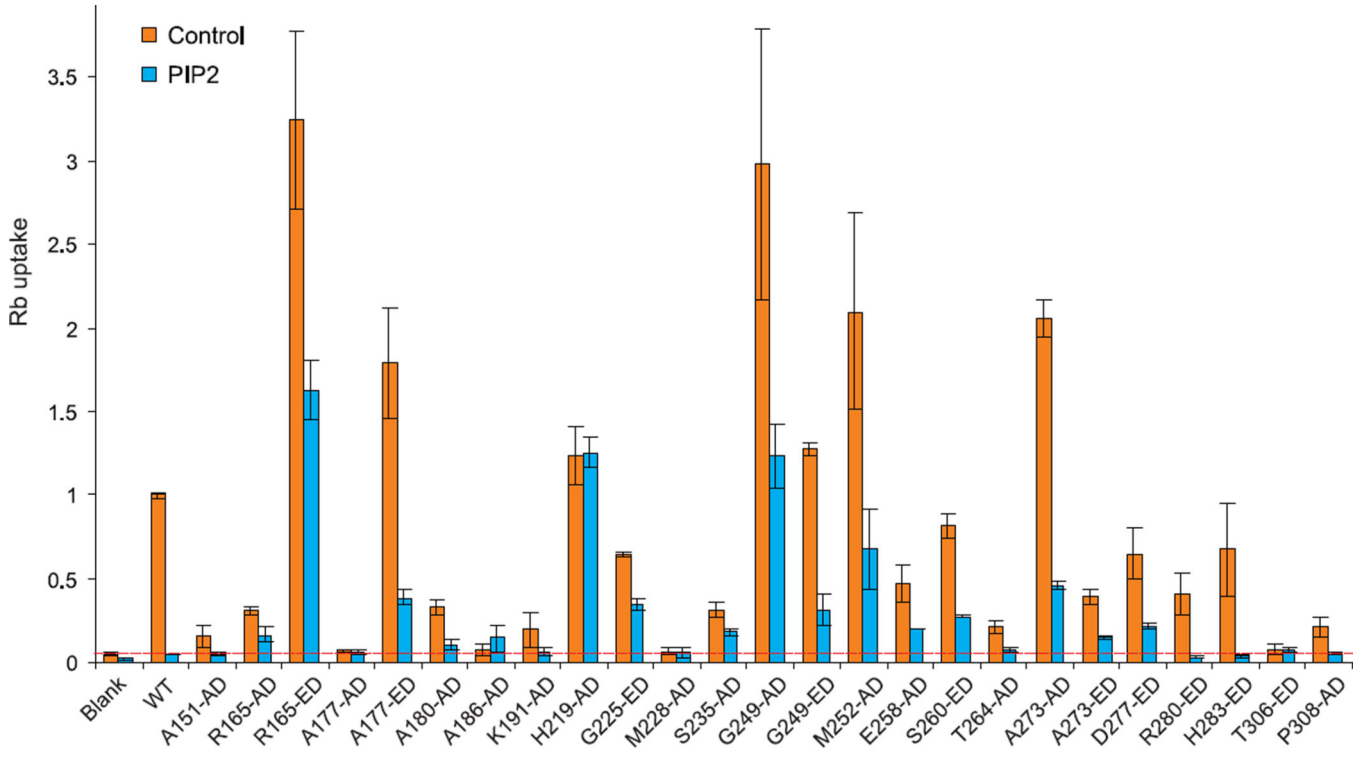

Fig. 2. Functional analysis of fluorophore-labeled KirBac1.1 cysteine-substituted mutants

Fluorophore-labeled KirBac1.1 mutants were reconstituted into liposomes (POPE:POPG=3:1) with or without 1.25% PIP_2 at protein/lipid ratio of 1:100 (w/w). The intraliposome buffer was 10 mM HEPES, 450 mM KCl and 4 mM NMDG, pH7.5, and the extraliposome buffer was 10 mM HEPES, 50 mM KCl, 400 mM sorbitol and 4 mM NMDG, pH7.5. $^{86}Rb^+$ uptake was measured at 15 min and normalized against the maximal $^{86}Rb^+$ uptake in the presence of valinomycin (Rb uptake). $^{86}Rb^+$ uptake of fluorophore-labeled mutants is shown as $^{86}Rb^+$ flux relative to wild type (mean±S.E, n=3 in each case). Background level of $^{86}Rb^+$ uptake (in liposomes with no protein) is marked by a red dashed line.

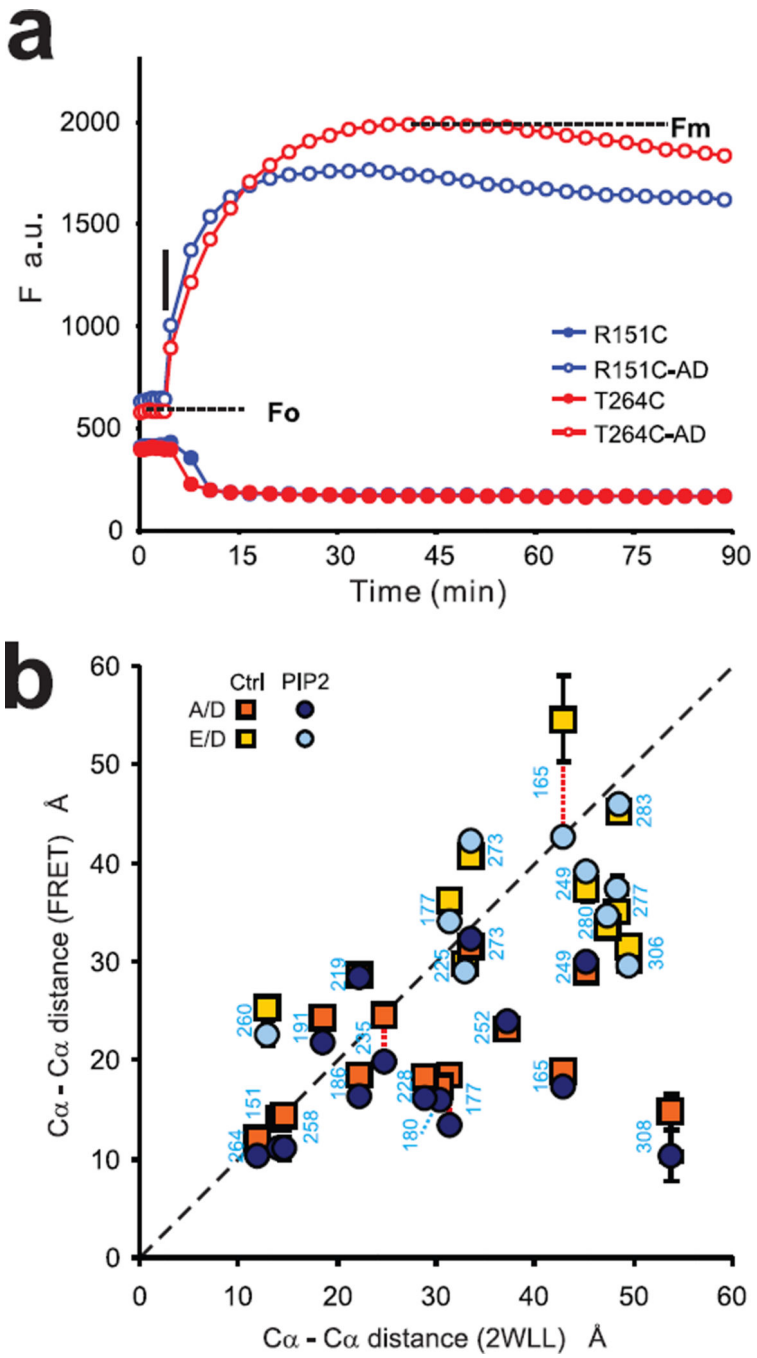

Fig. 3. FRET measurements reveal movements of individual residues during PIP_2 induced closure

(**a**) Representative time course of FRET measurements by proteinase K-mediated donor dequenching. KirBac1.1 R151C and T264C tetramers were labeled by A/D mixtures, then reconstituted into liposomes (POPE:POPG=3:1). Proteinase K (0.08U/well) was added after 8 repeated readings (F_o) (T=5 min); Alexa-Fluor-546 emission (F, a.u.) was monitored until emission reached maximum (F_{max}). (**b**) Cα-Cα distance between adjacent subunits of labeled residues predicted by FRET (mean±S.E, n=6–9 in each case) versus those present in

the KirBac1.1 (2WLL) crystal structure. R and p values of correlation are 0.51 ($p<0.010$), 0.54 ($p<0.006$) for Cα-Cα distances calculated from measured FRET efficiencies in the absence (control) and presence of 1.25% PIP_2, respectively.

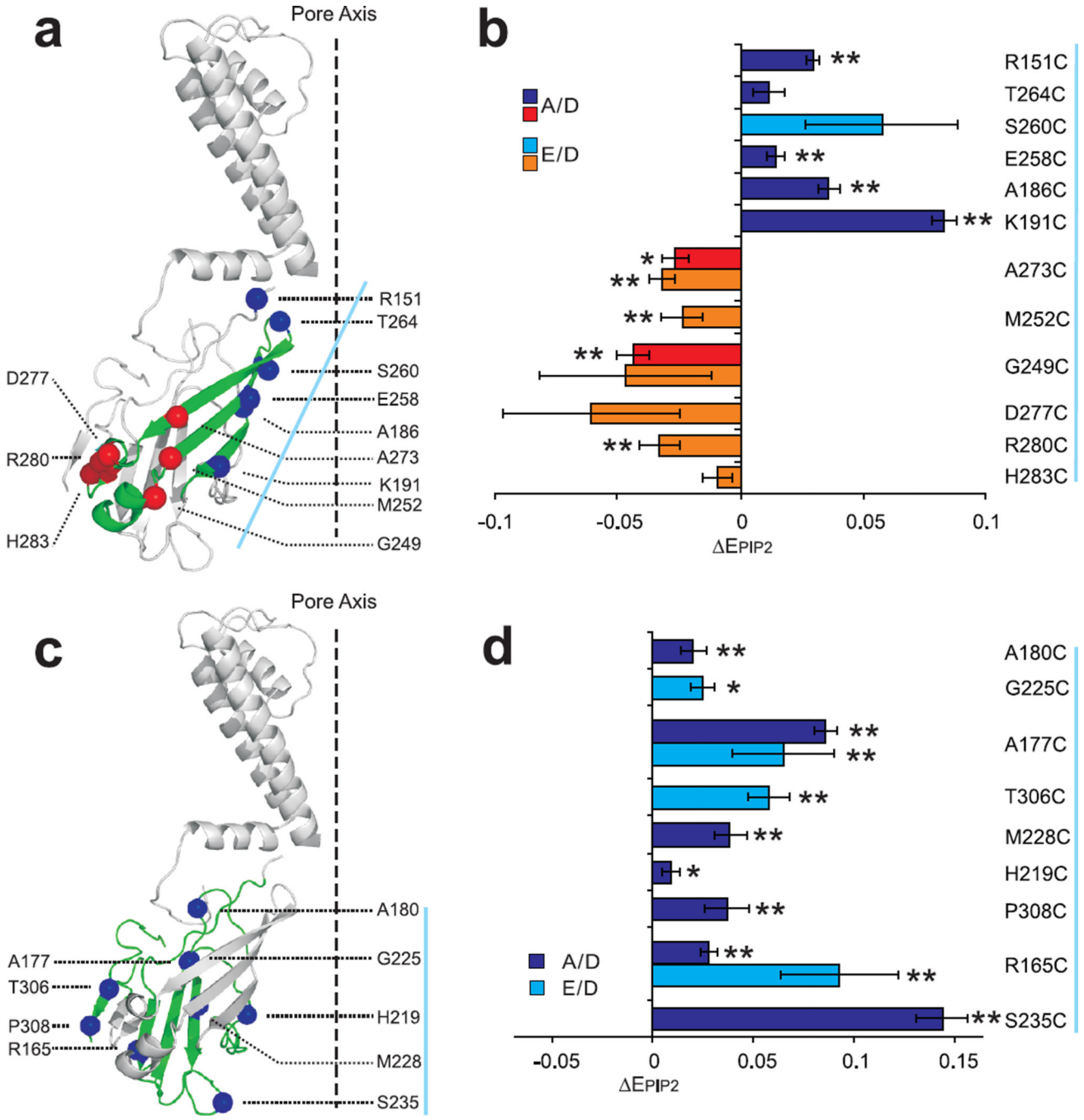

Fig. 4. Mapping FRET changes of individual residues to KirBac1.1 crystal structure suggest specific motions during gating

Changes of apparent FRET efficiencies of KirBac1.1 cysteine mutants in the large β-sheet (βI, panel **a** and **b**, green) and small β-sheets (βII and associated loops, panel **c** and **d**, green) in presence versus absence of PIP_2 (ΔE_{PIP2}, mean±S.E., n=6–9 in each case). Cα of the labeled residue is highlighted by spheres; residues demonstrating inward motion in the presence of PIP_2 are colored blue, those demonstrating outward motion are colored red; the

pore axis of KirBac1.1 is marked by dashed black line; amino acid residues in panels **b** and **d** are listed from top to bottom, along the axis indicated by a solid blue line.

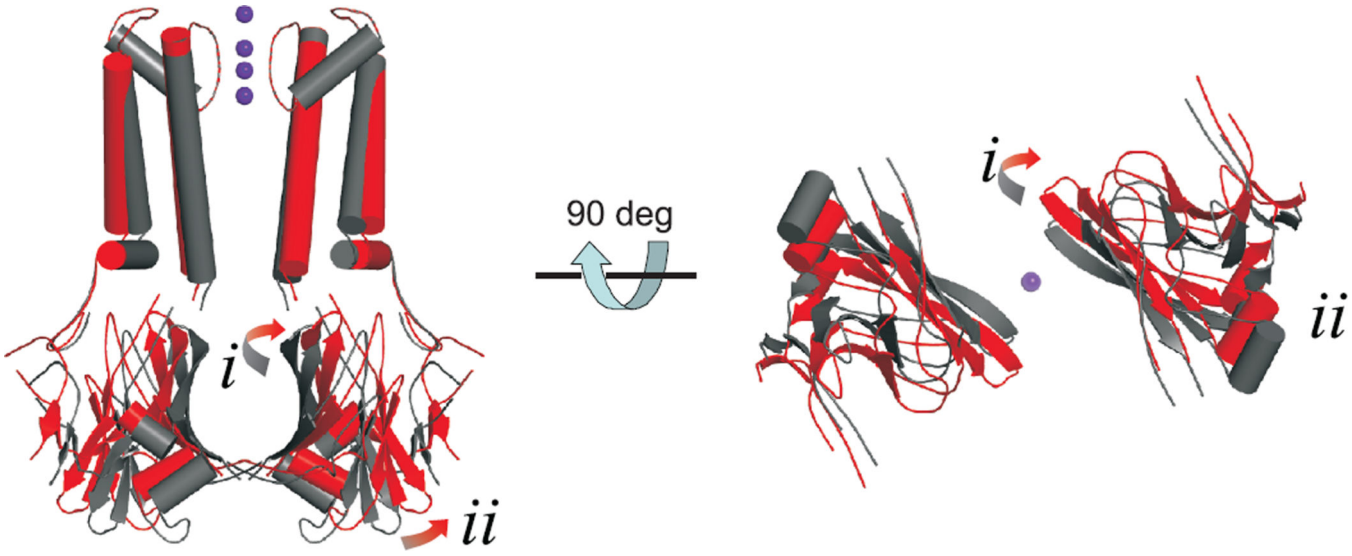

Fig. 5. 'Cartoon' model of ligand-gating of Kir channels

Views of closed (1P7B, gray) and 'open' (red) models of KirBac1.1 in (left) and from below (right) the plane of the membrane. Opening requires (***i***) outward twisting and tilting of βI, and (***ii***) outward motion of βII and associated short helices. For clarity, only two subunits are shown in each view.

Nat Commun. Author manuscript; available in PMC 2014 December 28.

Table 1

Changes of FRET efficiencies of labeled KirBac1.1 mutants in the presence or absence of PIP_2

	Control	PIP_2	ΔE	p	ΔE(Model)*
R151C-AD	0.855±0.002	0.885±0.002	+0.030	0.001	+
R165C-AD	0.788±0.002	0.816±0.003	+0.028	0.001	+
R165C-ED	0.054±0.029	0.147±0.004	+0.093	0.010	+
A177C-AD	0.794±0.005	0.880±0.002	+0.086	0.001	+
A177C-ED	0.286±0.010	0.351±0.023	+0.065	0.001	+
A180C-AD	0.815±0.003	0.835±0.005	+0.020	0.001	+
A186C-AD	0.795±0.003	0.831±0.003	+0.036	0.001	+
K191C-AD	0.628±0.004	0.711±0.002	+0.083	0.001	−
H219C-AD	0.463±0.004	0.472±0.001	+0.009	0.018	+
G225C-ED	0.483±0.003	0.508±0.005	+0.025	0.043	+
M228C-AD	0.796±0.008	0.835±0.002	+0.039	0.001	+
S235C-AD	0.619±0.010	0.763±0.008	+0.144	0.004	+
G249C-AD	0.451±0.002	0.407±0.006	−0.043	0.001	−
G249C-ED	0.260±0.033	0.213±0.011	−0.047	0.099	−
M252C-AD	0.668±0.003	0.644±0.008	−0.024	0.001	−
E258C-AD	0.853±0.002	0.868±0.003	+0.015	0.001	+
S260C-ED	0.616±0.014	0.674±0.028	+0.058	0.071	+
T264C-AD	0.886±0.001	0.898±0.006	+0.011	0.083	+
A273C-AD	0.350±0.005	0.324±0.002	−0.026	0.013	−
A273C-ED	0.184±0.005	0.153±0.001	−0.032	0.001	−
D277C-ED	0.321±0.022	0.261±0.028	−0.061	0.093	−
R280C-ED	0.362±0.007	0.329±0.005	−0.033	0.002	−
H283C-ED	0.111±0.006	0.102±0.001	−0.009	0.056	+
T306C-ED	0.427±0.005	0.485±0.009	+0.058	0.001	+
P308C-AD	0.837±0.010	0.874±0.004	+0.037	0.004	+

*Direction of FRET efficiency changes predicted by the ‘cartoon’ model of gating shown in Fig. 5, ‘+’ indicates increased FRET efficiency for closed versus open (see text). The FET efficiencies with (PIP_2) or without (Control) are presented as mean ± s.e.m, n=6.